Dynamical coupled-channels study of $\pi N \to \pi\pi N$ reactions

H. Kamano,[1] B. Juliá-Díaz,[1,2] T.-S. H. Lee,[1,3] A. Matsuyama,[1,4] and T. Sato[1,5]

[1]*Excited Baryon Analysis Center (EBAC), Thomas Jefferson National Accelerator Facility, Newport News, Virginia 23606, USA*
[2]*Department d'Estructura i Constituents de la Matèria and Institut de Ciències del Cosmos, Universitat de Barcelona E-08028 Barcelona, Spain*
[3]*Physics Division, Argonne National Laboratory, Argonne, Illinois 60439, USA*
[4]*Department of Physics, Shizuoka University, Shizuoka 422-8529, Japan*
[5]*Department of Physics, Osaka University, Toyonaka, Osaka 560-0043, Japan*

As a step toward performing a complete coupled-channels analysis of the world data of $\pi N, \gamma^* N \to \pi N, \eta N, \pi\pi N$ reactions, the $\pi N \to \pi\pi N$ reactions are investigated starting with the dynamical coupled-channels model developed in Phys. Rev. C **76**, 065201 (2007). The channels included are $\pi N, \eta N$, and $\pi\pi N$ which has $\pi\Delta, \rho N$, and σN resonant components. The nonresonant amplitudes are generated from solving a set of coupled-channels equations with the meson-baryon potentials defined by effective Lagrangians. The resonant amplitudes are generated from 16 bare excited nucleon (N^*) states that are dressed by the nonresonant interactions as constrained by the unitarity condition. The data of total cross sections and πN and $\pi\pi$ invariant mass distributions of $\pi^+ p \to \pi^+\pi^+ n, \pi^+\pi^0 p$ and $\pi^- p \to \pi^+\pi^- n, \pi^-\pi^0 p, \pi^0\pi^0 n$ reactions from threshold to the invariant mass $W = 2$ GeV can be described to a very large extent. We show the importance of the coupled-channels effects and the strong interference among the contributions from the $\pi\Delta, \sigma N$, and ρN channels. The large interference between the resonant and nonresonant amplitudes is also demonstrated. Possible future developments are discussed.

I. INTRODUCTION

It has been well recognized [1] that a coupled-channels analysis of the data of meson production from $\pi N, \gamma N$, and $N(e, e')$ reactions is needed to extract the parameters of the excited nucleon (N^*) states in the energy region above the $\Delta(1232)$ resonance. This has been pursued by using K-matrix models [2–5], the Carnegie-Mellon-Berkeley (CMB) model [6], and dynamical models [7–16]. Since two-pion production processes account for about half of the total cross sections of πN and γN reactions, the N^* parameters extracted from these analyses are reliable only when the employed models are consistent with the two-pion production data. As a step toward performing a complete analysis of the world data of $\pi N, \gamma^* N \to \pi N, \eta N, \pi\pi N$ reactions, we investigate in this paper the $\pi N \to \pi\pi N$ reaction starting with the dynamical coupled-channels model developed in Ref. [13] (JLMS) from fitting the πN elastic scattering data.

A number of theoretical investigations of $\pi N \to \pi\pi N$ reactions have been performed using (1) tree-diagram calculations [17–23], (2) chiral perturbation theory [24–27], and (3) tree-diagram calculations including coupled-channels effects on nucleon resonances [28]. To see the scope of our investigation, it is useful to give a brief review of these previous works in the following sections.

A. Tree-diagram calculations

The tree-diagram calculations are based on phenomenological Lagrangians and the Breit-Wigner form parametrization of nucleon resonances. All $\pi^\pm p \to \pi\pi N$ channels on the proton target were investigated in Refs. [21–23], whereas only

the $\pi^- p \to \pi^+\pi^- n$ channel was studied in Refs. [17–20]. These investigations covered the energy region up to invariant mass $W = 1551$ MeV ($T_\pi = 600$ MeV) and only investigated the role of the $\Delta(1232)$ and $N^*(1440)$ resonances. They could describe reasonably well the experimental data in the considered energy region. An attempt was also made to investigate the scalar-isoscalar two-pion decay process of $N^*(1440) \to N(\pi\pi)_{\text{S wave}}^{I=0}$ of the Roper resonance. Although the tree-diagram calculation is a convenient tool to catch the qualitative features of the reaction processes, it is of course not consistent with the unitarity requirements. Furthermore, such an approach starts to break down in the $W \gtrsim 1.5$ GeV region, where more N^* states needed to be considered.

B. Chiral perturbation theory

Chiral perturbation theory calculations of $\pi N \to \pi\pi N$ reactions have been performed up to $O(q^3)$. The focus of Ref. [24] was on evaluating the $\pi N \to \pi\pi N$ threshold amplitudes $D_{1,2}$ and extracting the $\pi\pi$ scattering length within heavy-baryon chiral perturbation theory. This work was extended in Refs. [25,26] to also compare with the cross section data up to $W = 1.38$ GeV ($T_\pi = 400$ MeV). It was found that the loop corrections are small and it is difficult to extract the isoscalar S-wave $\pi\pi$ scattering length because of the large uncertainty associated with the $N^*(1440) \to N(\pi\pi)_{\text{S wave}}^{I=0}$ decay. A similar chiral perturbation theory calculation was also performed to compare with more data near the threshold by Mobed *et al.* [27].

Of course, the application of chiral perturbation theory to investigate the $\pi N \to \pi\pi N$ reactions near threshold is an

important advance, but it is not clear how it can be used to investigate nucleon resonances up to $W = 2$ GeV.

C. Tree-diagram calculation including coupled-channels effects on N^*

The $\pi N \to \pi \pi N$ study performed by the Julich group [28] also used the tree diagrams generated from phenomenological Lagrangians, but including the $P_{33}(1232)$, $P_{11}(1440)$, $D_{13}(1520)$, $S_{11}(1535)$, and $S_{11}(1650)$ resonance states. They focused on the low $W \leqslant 1.38$ GeV ($T_\pi = 400$ MeV) region. The coupled-channels effects are included by using the nonresonant amplitudes generated from the πN coupled-channels model of Ref. [8] to evaluate the self-energy and the decay functions of the considered resonances. They could describe to a large extent most of the available data in the $W < 1.38$ GeV region. They found that their calculations started to break down in the higher W region.

In this work, we depart from all of the earlier works just described by considering the whole energy region from threshold up to $W = 2$ GeV and all nucleon resonances listed by the Particle Data Group (PDG) [29]. The calculations are performed by using the JLMS model. Schematically, the following coupled integral equations in each partial wave are solved within the JLMS model:

$$T_{\alpha,\beta}(p_\alpha, p_\beta; E) = V_{\alpha,\beta}(p_\alpha, p_\beta) + \sum_\delta \int p^2 dp\, V_{\alpha,\delta}(p_\alpha, p)$$
$$\times\, G_\delta(p, E) T_{\delta,\beta}(p, p_\beta, E), \tag{1}$$

with

$$V_{\alpha,\beta}(p_\alpha, p_\beta) = v_{\alpha,\beta}(p_\alpha, p_\beta) + \sum_{N^*} \frac{\Gamma^\dagger_{N^*,\alpha}(p_\alpha)\Gamma_{N^*,\beta}(p_\beta)}{E - M^0_{N^*}}, \tag{2}$$

where $\alpha, \beta, \delta = \gamma N, \pi N, \eta N$, and $\pi \pi N$, which has $\pi \Delta$, ρN, σN resonant components, $G_\delta(p, E)$ is the propagator of channel δ, $M^0_{N^*}$ is the mass of a bare excited nucleon state N^*, $v_{\alpha,\beta}$ is defined by meson-exchange mechanisms, and the vertex interaction $\Gamma_{N^*,\beta}$ defines the $N^* \to \beta$ decay. The fits to πN elastic scattering data were achieved by including one or two bare N^* states in all S, P, D, and F partial waves. The details can be found in Ref. [13].

Although the nonresonant interactions $v_{\alpha,\beta}$ are deduced from phenomenological Lagrangians, the model contains many parameters mainly because of the lack of sound theoretical guidance in parametrizing the bare $N^* \to \pi N, \eta N, \pi \Delta, \rho N, \sigma N$ form factors. Although fitting the πN elastic scattering data is rather complex and time consuming, as reported in Ref. [13], it is clearly not sufficient to determine these parameters, in particular the parameters associated with the unstable $\pi \Delta$, ρN, and σN channels. Thus it is important to test the JLMS model in the study of $\pi N \to \pi \pi N$ reactions, which are known to be dominated by these channels. This is the main purpose of this work. The results presented in this paper are therefore obtained by using the parameters taken from the JLMS model.

It is tempting to try to use the available $\pi N \to \pi \pi N$ data to improve the JLMS model. However, this is not an easy task at the present time mainly because of the lack of sufficient

experimental data in the considered energy region up to $W = 2$ GeV ($T_\pi \sim 1.6$ GeV). Furthermore, most of the data at high W, obtained before the 1970s, are not accessible [30]. In an effort by Arndt [30], some of the final $\pi \pi$ and πN invariant mass distribution data have been recovered and considered in this paper along with the most studied total cross section data [31]. This allows us to investigate these two observables for all possible final $\pi \pi N$ states of $\pi^\pm p$ reactions and in the entire energy region from threshold to $W = 2$ GeV. Very limited data on the angular distributions can be found in the literature, with only a few in the low-W region and practically nothing in the higher W region where we need pin down the parameters associated with many N^* states. We thus will not consider these observables. For the same reason it is difficult to use the available $\pi N \to \pi \pi N$ data at the present time. This is mainly due to the problem that the minimization in determining a large amount of parameters of our model is heavily weighted by the very extensive and far more precise data of πN elastic scattering. We thus focus in this paper on investigating the dynamical content of the JLMS model, in particular on several aspects that were not addressed before, such as the effects of coupled channels and the role played by the interference between the different channels. Even with this limitation our investigation is clearly more extensive than all previous works just reviewed.

In Sec. II, we briefly recall the formulas of Ref. [12] for calculating the $\pi N \to \pi \pi N$ amplitudes within the JLMS model. To give more details about our calculations, explicit expressions for calculating the total cross sections and πN and $\pi \pi$ invariant mass distributions are given in Sec. III. The results are presented in Sec. IV. In Sec. V, we give a summary and discuss possible future developments.

II. FORMULATION

Within a Hamiltonian formulation [12] within which the JLMS model was developed, the $\pi N \to \pi \pi N$ amplitude is illustrated in Fig. 1 and can be written as

$$T_{\pi N, \pi \pi N}(E) = T^{\text{dir}}_{\pi N, \pi \pi N}(E) + T^{\pi \Delta}_{\pi N, \pi \pi N}(E)$$
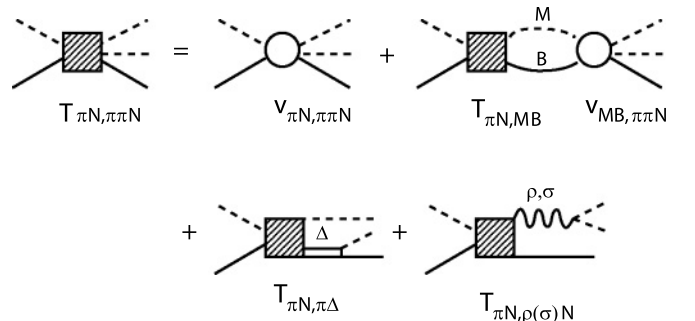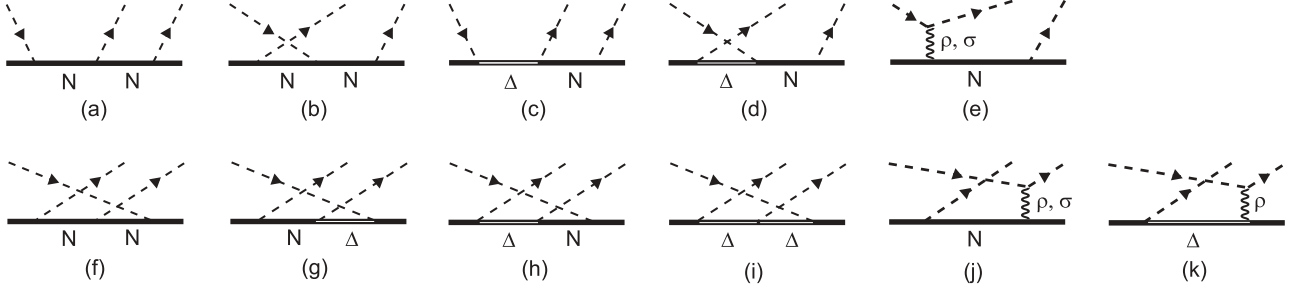$$+ T^{\rho N}_{\pi N, \pi \pi N}(E) + T^{\sigma N}_{\pi N, \pi \pi N}(E), \tag{3}$$

FIG. 1. Graphical representations of $T_{\pi N, \pi \pi N}$ of Eqs. (3)–(7).

FIG. 2. The considered $v_{\pi N, \pi\pi N}$.

with

$$T_{\pi N, \pi\pi N}^{\text{dir}}(E) = v_{\pi N, \pi\pi N}$$
$$+ \sum_{MB} T_{\pi N, MB}(E) G_{MB}(E) v_{MB, \pi\pi N}, \quad (4)$$

$$T_{\pi N, \pi\pi N}^{\pi\Delta}(E) = T_{\pi N, \pi\Delta}(E) G_{\pi\Delta}(E) \Gamma_{\Delta \to \pi N}, \quad (5)$$

$$T_{\pi N, \pi\pi N}^{\rho N}(E) = T_{\pi N, \rho N}(E) G_{\rho N}(E) h_{\rho \to \pi\pi}, \quad (6)$$

$$T_{\pi N, \pi\pi N}^{\sigma N}(E) = T_{\pi N, \sigma N}(E) G_{\sigma N}(E) h_{\sigma \to \pi\pi}, \quad (7)$$

where $\Gamma_{\Delta \to \pi N}$, $h_{\rho \to \pi\pi}$, and $h_{\sigma \to \pi\pi}$ describe the $\Delta(1232) \to \pi N$, $\rho \to \pi\pi$, and $\sigma \to \pi\pi$ decays, respectively, and $G_{MB}(E)$ for $MB = \pi N, \eta N, \pi\Delta, \rho N$, and σN are the meson-baryon propagators. The $\pi N \to MB$ transition amplitudes are

$$T_{\pi N, MB}(E) = t_{\pi N, MB}(E) + t_{\pi N, MB}^R(E). \quad (8)$$

The second term on the right-hand-side of Eq. (8) is the resonant term defined by

$$t_{MB, M'B'}^R(E) = \sum_{N_i^*, N_j^*} \bar{\Gamma}_{MB \to N_i^*}(E) [D(E)]_{i,j} \bar{\Gamma}_{N_j^* \to M'B'}(E), \quad (9)$$

with

$$[D(E)^{-1}]_{i,j}(E) = (E - M_{N_i^*}^0) \delta_{i,j} - \bar{\Sigma}_{i,j}(E), \quad (10)$$

where $M_{N^*}^0$ is the bare mass of the excited nucleon state N^*, and the self-energies are

$$\bar{\Sigma}_{i,j}(E) = \sum_{MB} \Gamma_{N_i^* \to MB} G_{MB}(E) \bar{\Gamma}_{MB \to N_j^*}(E). \quad (11)$$

Defining $\Gamma_{MB \to N^*} = \Gamma_{N^* \to MB}^\dagger$ we have that the dressed vertex interactions in Eq. (9) and Eq. (11) are

$$\bar{\Gamma}_{MB \to N^*}(E) = \Gamma_{MB \to N^*}$$
$$+ \sum_{M'B'} t_{MB, M'B'}(E) G_{M'B'}(E) \Gamma_{M'B' \to N^*}, \quad (12)$$

$$\bar{\Gamma}_{N^* \to MB}(E) = \Gamma_{N^* \to MB}$$
$$+ \sum_{M'B'} \Gamma_{N^* \to M'B'} G_{M'B'}(E) t_{M'B', MB}(E). \quad (13)$$

The nonresonant amplitudes $t_{MB, M'B'}$ in Eq. (8) and Eqs. (12) and (13) are defined by the following coupled-channels equations:

$$t_{MB, M'B'}(E) = v_{MB, M'B'} + \sum_{M''B''} v_{MB, M''B''}$$

$$\times G_{M''B''}(E) t_{M''B'', M'B'}(E). \quad (14)$$

The channels included are $MB = \pi N, \eta N, \pi\Delta, \rho N$, and σN. All quantities defined here are described in detail in Refs. [12,13] and can be calculated within the JLMS model. The only exception is the direct production term $v_{\pi N, \pi\pi N}$ in Eq. (4), which is not included in the JLMS model. The procedure for deriving $v_{\pi N, \pi\pi N}$ from Lagrangians by using the method of unitary transformation is explained in Ref. [12]. In this work we consider a $v_{\pi N, \pi\pi N}$ model, which involves only the N and $\Delta(1232)$ intermediate baryon states such that its parameters can also be consistently taken from the JLMS model. Our calculations thus do not have any adjustable parameters. The mechanisms of the considered $v_{\pi N, \pi\pi N}$ are illustrated in Fig. 2.

The calculations of the terms $T_{\pi N, \pi\pi N}^{MB}$ with $MB = \pi\Delta, \rho N, \sigma N$, defined by Eqs. (5)–(7), are straightforward. However, the calculation of the second term of $T_{\pi N, \pi\pi N}^{\text{dir}}$, defined by Eq. (4), is much more complex. To simplify the calculation, we first note that the mechanisms (a)–(e) in the upper row of Fig. 2 can be written as

$$v_{\pi N, \pi\pi N}^{(\text{a–e})} \sim v_{\pi N, \pi N} G_{\pi N}(E) h_{N \to \pi N}, \quad (15)$$

where $v_{\pi N, \pi\pi N}^{(\text{a–e})}$ is the sum of all mechanisms (a)–(e), $v_{\pi N, \pi N}$ is part of the driving term in calculating the amplitude $T_{\pi N, \pi N}(E)$ from the JLMS model, and $h_{N \to \pi N}$ is the $N \to \pi N$ vertex function. If we neglect the final state interactions on the mechanisms (f)–(k) of Fig. 2, we can write

$$T_{\pi N, \pi\pi N}^{\text{dir}} \sim v_{\pi N, \pi\pi N}^{(\text{f–k})} + \left[v_{\pi N, \pi N} + \sum_{MB} T_{\pi N, MB}(E) G_{MB}(E) \right.$$

$$\left. \times v_{MB, \pi N} \right] G_{\pi N}(E) h_{N \to \pi N}$$

$$\sim v_{\pi N, \pi\pi N}^{(\text{f–k})} + T_{\pi N, \pi N}(E) G_{\pi N}(E) h_{N \to \pi N}. \quad (16)$$

In deriving this equation, we have used the full scattering equation $T = V + TGV$ of the JLMS model. We use Eq. (16) in this work.

III. CROSS-SECTION FORMULA

For presenting results, we here give explicit formulas for calculating the cross sections of $\pi N \to \pi\pi N$ reactions. Within the formulation of Refs. [12,13], the S matrix is defined

by

$$S_{fi} = \delta_{fi} - 2\pi i \delta^4(P_f - P_i)\langle f|T|i\rangle, \qquad (17)$$

and the plane-wave state is normalized as

$$\langle \vec{q}|\vec{p}\rangle = \delta(\vec{q} - \vec{p}). \qquad (18)$$

In the center-of-mass frame, the momentum variables of the $\pi N \to \pi\pi N$ reaction with invariant mass W can be specified as

$$a(\vec{p}_a) + b(\vec{p}_b) \to c(\vec{p}_c) + d(\vec{p}_d) + e(\vec{p}_e), \qquad (19)$$

where $\vec{p}_a = -\vec{p}_b = \vec{k}$ with k defined by $W = E_a(k) + E_b(k)$, $\vec{p}_c + \vec{p}_d = -\vec{p}_e = \vec{k}'$, and $(c + d + e)$ can be any possible charged states formed from two pions and one nucleon. The total cross section of the process [Eq. (19)] can then be written as

$$\sigma_{ab\to cde} = \frac{1}{v}(2\pi)^4 \int d\vec{p}_c d\vec{p}_d d\vec{p}_e \delta^4(p_a + p_b - p_c - p_d - p_e)$$
$$\times \frac{1}{(2s_a + 1)(2s_b + 1)} \sum_{\bar{i},\bar{f}} |\langle \vec{p}_c \vec{p}_d \vec{p}_e, f|T|\vec{p}_a \vec{p}_b, i\rangle|^2$$
$$= \frac{E_a(k)E_b(k)}{Wk}(2\pi)^4 \int \frac{d\vec{p}_c}{E_c} \frac{d\vec{p}_d}{E_d} \frac{d\vec{p}_e}{E_e}$$
$$\times \delta^4(p_a + p_b - p_c - p_d - p_e)\frac{1}{(2s_a + 1)(2s_b + 1)}$$
$$\times \sum_{\bar{i},\bar{f}} |\sqrt{E_c E_d E_e}\langle \vec{p}_c \vec{p}_d \vec{p}_e, f|T|\vec{p}_a \vec{p}_b, i\rangle|^2, \qquad (20)$$

where i, f denote all spin (s_a, s_{az}) and isospin (t_a, t_{az}) quantum numbers, and $\sum_{\bar{i},\bar{f}}$ means summing over only spin quantum numbers. This equation can be written as

$$\sigma_{ab\to cde} = \int_{m_c+m_d}^{W-m_e} \frac{d\sigma}{dM_{cd}}dM_{cd}, \qquad (21)$$

with

$$\frac{d\sigma}{dM_{cd}} = \frac{\rho_i}{k^2}16\pi^3 \int d\Omega_{k_{cd}}d\Omega_{k'}\frac{k_{cd}k'}{W}\frac{1}{(2s_a + 1)(2s_b + 1)}$$
$$\times \sum_{\bar{i},\bar{f}} |\sqrt{E_c E_d E_e}\langle \vec{p}_c \vec{p}_d \vec{p}_e, f|T|\vec{k}, i\rangle|^2. \qquad (22)$$

Here we have defined

$$\rho_i = \pi \frac{k E_a(k)E_b(k)}{W},$$
$$W = E_e(k') + E_{cd}(k'),$$
$$E_{cd}(k') = \sqrt{M_{cd}^2 + (k')^2}, \qquad (23)$$
$$M_{cd} = E_c(k_{cd}) + E_d(k_{cd}),$$

and $\vec{k}_{cd}$ is the relative momentum between c and d in the e rest frame.

The T-matrix elements in this equation are calculated from Eqs. (4)–(7). For the quasi-two-body processes given by Eqs. (5)–(7) with a resonant unstable particle R, which decays into the $c + d$ state, the T-matrix elements take the following

form:

$$\langle p_c \vec{p}_d \vec{p}_e, f|T|\vec{k}, i\rangle$$
$$= \sum_{s_{R_z}, t_{R_z}} \frac{\langle \vec{p}_c, s_{cz}, t_{cz}; \vec{p}_d, s_{dz}, t_{dz}|H_I|\vec{k}', s_{R_z}, t_{R_z}\rangle}{E - E_e(k') - E_R(k') - \Sigma_{eR}(k', W)}$$
$$\times \langle \vec{k}', s_{R_z}, t_{R_z}; -\vec{k}', s_{ez}, t_{ez}|T|\vec{k}, s_{az}, t_{az}; -\vec{k}, s_{bz}, t_{bz}\rangle. \qquad (24)$$

For any spins and isospins and center-of-mass momenta $\vec{p}$ and $\vec{p}'$, the $MB \to M'B'$ T-matrix elements are in general defined by

$$\langle \vec{p}', s_{M'z}, t_{M'z}; -\vec{p}', s_{B'z}, t_{B'z}|T|\vec{p}, s_{Mz}, t_{Mz}; -\vec{p}, s_{Bz}, t_{Bz}\rangle$$
$$= \sum_{S,S',L,L',J,M,I} Y_{L',M'_L}(\hat{p}')Y^*_{L,M_L}(\hat{p})$$
$$\times \langle s_{M'}, s_{M'z}, s_{B'}, s_{B'z}|S', S'_z\rangle\langle L', M'_L, S', S'_z|J, M\rangle$$
$$\times \langle t_{M'}, t_{M'z}, t_{B'}, t_{B'z}|I, I_z\rangle\langle s_M, s_{Mz}, s_B, s_{Bz}|S, S_z\rangle$$
$$\times \langle L, M_L, S, S_z|J, M\rangle\langle t_M, t_{Mz}, t_B, t_{Bz}|I, I_z\rangle$$
$$\times \langle p', S'L'J|T^I(W)|p, SLJ\rangle, \qquad (25)$$

where $\langle j_1, j_1, m_1, m_2|jm\rangle$ is the Clebsch-Gordan coefficient of the $j_1 + j_2 = j$ coupling, and $\langle k', S'L'J|T^I(W)|k, SLJ\rangle$ is the partial wave amplitude defined by the total angular momentum J, orbital angular momentum L, total spin S, and total isospin I. We use the JLMS model to generate $\langle k', S'L'J|T^I(W)|k, SLJ\rangle$.

As for the $R \to cd$ vertex function, the combination

$$\sqrt{E_c(p_c)E_d(p_d)E_R(k')}$$
$$\times \langle \vec{p}_c, s_{cz}, t_{cz}; \vec{p}_d, s_{dz}, t_{dz}|H_I|\vec{k}', s_{R_z}, t_{R_z}\rangle \qquad (26)$$

is Lorentz invariant and therefore can be written in terms of its matrix element in the rest frame of R:

$$\langle \vec{p}_c, s_{cz}, t_{cz}; \vec{p}_d, s_{dz}, t_{dz}|H_I|\vec{k}', s_{R_z}, t_{R_z}\rangle$$
$$= \delta(\vec{p}_c + \vec{p}_d - \vec{k}')\sqrt{\frac{E_c(k_{cd})E_d(k_{cd})M_R}{E_c(p_c)E_d(p_d)E_R(k')}}$$
$$\times \langle \vec{k}_{cd}, s_{cz}, t_{cz}; -\vec{k}_{cd}, s_{dz}, t_{dz}|H_I|\vec{0}, s_{R_z}, t_{R_z}\rangle, \qquad (27)$$

with

$$\langle \vec{k}_{cd}, s_{cz}, t_{cz}; -\vec{k}_{cd}, s_{dz}, t_{dz}|H_I|\vec{0}, s_{R_z}, t_{R_z}\rangle$$
$$= \sum_{L_{cd}, m_{cd}, S_{cd}, S_{cdz}} [\langle s_c, s_{cz}, s_d, s_{dz}|S_{cd}, S_{cdz}\rangle$$
$$\times \langle L_{cd}, m_{cd}, S_{cd}, S_{cdz}|s_R, s_{R_z}\rangle\langle t_c, t_{cz}, t_d, t_{dz}|t_R, t_{R_z}\rangle$$
$$\times Y_{L_{cd}, m_{cd}}(\hat{k}_{cd})F^R_{L_{cd}, S^R_{cd}}(k_{cd})]. \qquad (28)$$

The vertex functions are

$$F_{L^\Delta_{\pi N}, S^\Delta_{\pi N}}(q) = if_{\Delta\to\pi N}(q), \qquad (29)$$

$$F_{L^\sigma_{\pi\pi}, S^\sigma_{\pi\pi}}(q) = \sqrt{2}f_{\sigma\to\pi\pi}(q), \qquad (30)$$

$$F_{L^\rho_{\pi\pi}, S^\rho_{\pi\pi}}(q) = (-1)\sqrt{2}f_{\rho\to\pi\pi}(q), \qquad (31)$$

where $L^\Delta_{\pi N} = 1$, $S^\Delta_{\pi N} = 3/2$, $L^\sigma_{\pi\pi} = 0$, $S^\sigma_{\pi\pi} = 0$, and $L^\rho_{\pi\pi} = 1$, $S^\rho_{\pi\pi} = 1$. Here it is noted that the factor $\sqrt{2}$ in Eqs. (30) and (31) comes from the Bose symmetry of pions, and the phase factor i and (-1) are chosen to be consistent with the nonresonant interactions involving $\pi N \Delta$, $\sigma\pi\pi$, and $\rho\pi\pi$
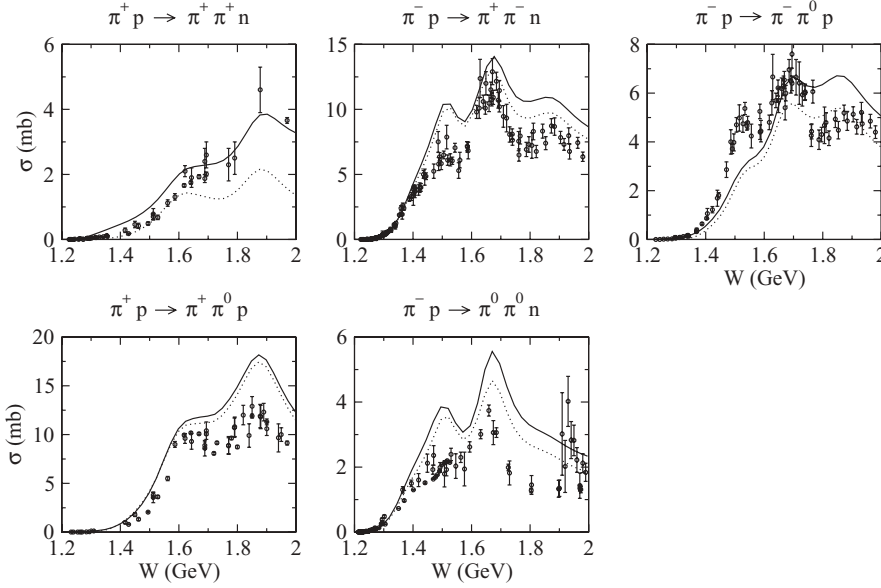
FIG. 3. The total cross sections predicted (solid curves) from the JLMS model compared with the data [31]. The dotted curves are from turning off the amplitude $T^{\mathrm{dir}}_{\pi N, \pi\pi N}$.

vertex interactions defined in Ref. [12]. The form factors in Eqs. (30) and (31) are

$$f_{\Delta \to \pi N}(q) = -\frac{f_{\pi N\Delta}}{m_\pi} \frac{1}{(2\pi)^{3/2}} \sqrt{\frac{4\pi}{3}} q \frac{1}{\sqrt{2E_\pi(q)}}$$
$$\times \sqrt{\frac{E_N(q) + m_N}{2E_N(q)}} \left(\frac{\Lambda^2_{\pi N\Delta}}{\Lambda^2_{\pi N\Delta} + q^2} \right)^2, \quad (32)$$

$$f_{\sigma \to \pi\pi}(q) = \frac{g_{\sigma\pi\pi}}{\sqrt{m_\pi}} \frac{\Lambda^2_{\sigma\pi\pi}}{\Lambda^2_{\sigma\pi\pi} + q^2}, \quad (33)$$

$$f_{\rho \to \pi\pi}(q) = \frac{g_{\rho\pi\pi}}{\sqrt{m_\pi}} \frac{q}{\Lambda_{\rho\pi\pi}} \left(\frac{\Lambda^2_{\rho\pi\pi}}{\Lambda^2_{\rho\pi\pi} + q^2} \right)^2, \quad (34)$$

with $f_{\pi N\Delta} = 2.049$, $g_{\sigma\pi\pi} = 0.7750$, $g_{\rho\pi\pi} = 0.6684$, $\Lambda_{\pi N\Delta} = 649$ MeV, $\Lambda_{\sigma\pi\pi} = 378$ MeV, and $\Lambda_{\rho\pi\pi} = 461$ MeV. These vertex functions are determined from fitting the πN phase shifts in P_{33} [32] and $\pi\pi$ phase shifts [33].

With the vertex function $f_{R \to cd}(q)$ as given here, the self-energy appearing in the eR Green function, $\Sigma_{eR}(eR = \pi\Delta, N\rho, N\sigma)$, is calculated from (see Appendix A)

$$\Sigma_{eR}(k, E) = \frac{m_R}{E_R(k)} \int q^2 dq \frac{M_{eR}(q)}{\left[M^2_{eR}(q) + k^2 \right]^{1/2}}$$
$$\times \frac{|f_{R \to cd}(q)|^2}{E - E_e(k) - \{[E_c(q) + E_d(q)]^2 + k^2\}^{1/2} + i\varepsilon}. \quad (35)$$

To derive this equation, we have used the Lorentz transformation to calculate the self-energy in an arbitrary frame from the vertex function defined in the rest frame of R.

IV. RESULTS

With the formula presented in Secs. II and III, we now present results for the total cross sections $\sigma_{\pi N \to \pi\pi N}$ and the invariant mass distributions $d\sigma/dM_{\pi N}$ or $d\sigma/dM_{\pi\pi}$ for all possible final $\pi\pi N$ states of $\pi^\pm p$ reactions in the energy

region from threshold to invariant mass $W = 2$ GeV. As mentioned in Sec. I, our investigation thus is much more extensive than all of the previous dynamical calculations of $\pi N \to \pi\pi N$ reactions in both the energy range covered and the N^* states considered.

We can predict the $\pi N \to \pi\pi N$ cross sections using the information generated from the JLMS model except that due to the direct production interaction $v_{\pi N, \pi\pi N}$ in Eq. (4). This term, which can induce the $\pi N \to \pi\pi N \to \pi N$ mechanism to influence the πN elastic scattering, was not included in the development of the JLMS model. We thus first examine the importance of this term. As discussed in Sec. II, the contributions from $v_{\pi N, \pi\pi N}$, calculated by using $T^{\mathrm{dir}}_{\pi N, \pi\pi N}$ defined in Eq. (16), is completely fixed by using the same parameters from the JLMS model. Thus no additional parameters are introduced in our calculations.

Our results for the total cross sections are shown in Fig. 3. The solid curves are from our full calculations and the dashed curves are from turning off the term $T^{\mathrm{dir}}_{\pi N, \pi\pi N}$. We see that both the magnitudes and the energy dependence of the data for all five two-pion production processes can be reproduced to a very large extent by our full calculations (solid curves). Clearly, the direct $\pi N \to \pi\pi N$ mechanism plays a significant role in determining the predicted cross sections. In particular, it is instrumental in obtaining the agreement with the $\pi^+ p \to \pi^+\pi^+ n$ data. Its effects at low W can be more clearly seen in Fig. 4. Here we also see that the agreement with the data of $\pi^- p \to \pi^0\pi^- p$ is mainly due to the effects of $v_{\pi N, \pi\pi N}$. We note here that our full calculations (solid curves) in Fig. 4 are comparable to those of the chiral perturbation theory calculation of Refs. [25–27]. This suggests that the model $v_{\pi N, \pi\pi N}$ considered here is fairly reasonable and the discrepancies with the data in the higher W region, seen in Fig. 3, more likely result from the uncertainties in the contributions from $\pi\Delta$, σN, and ρN transitions.

The main feature of this investigation is a dynamical coupled-channels treatment of the $\pi\pi N$ channel, which has the $\pi\Delta$, ρN, and σN resonant channels. In our calculation, this
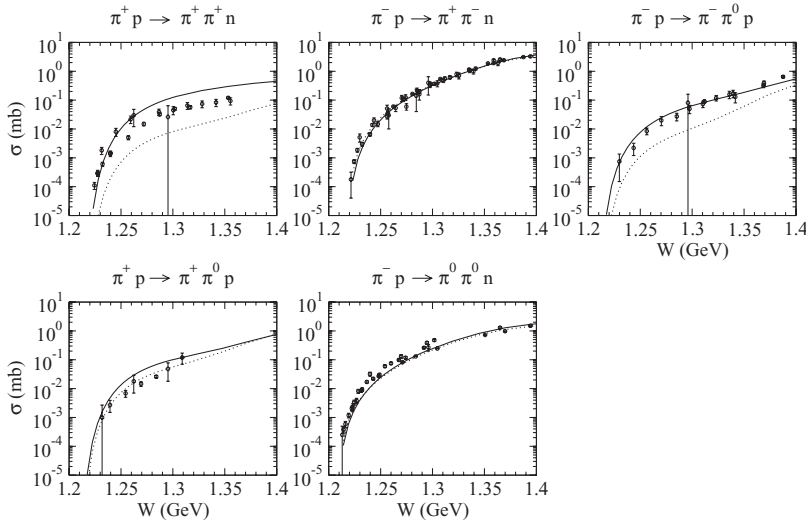
FIG. 4. The total cross sections predicted (solid curves) from the JLMS model compared with the data [31]. The dotted curves are from turning off the amplitude $T^{\mathrm{dir}}_{\pi N, \pi\pi N}$.

effect can be explicitly seen by writing the coupled-channels equations, Eq. (14), as

$$t_{\pi N, MB}(E) = \sum_{M'B'} [1 - vG]^{-1}_{\pi N, M'B'} v_{M'B', MB}, \qquad (36)$$

where $MB = \pi\Delta, \rho N, \sigma N$, and the intermediate meson-baryon states can be $M'B' = \pi N, \eta N, \pi\Delta, \sigma N, \rho N$. When only the term with $M'B' = MB$ in Eq. (36) and in $\bar{\Gamma}_{N^* \to MB}$ of Eqs. (12) and (13) is kept, the calculated total cross sections (full curves) are changed to the dotted curves in Fig. 5. If we further neglect the coupled-channels effects by setting $t_{\pi N, MB} = v_{\pi N, MB}$, we then get the dashed curves, which are very different from the full calculations (solid curves), in particular in the high-W region.

To see the coupled-channels effects more clearly, we show the corresponding results for the πN and $\pi\pi$ invariant mass distributions at $W = 1.79$ GeV in Figs. 6 and 7. Our full calculations (solid curves) are able to reproduce the main features of the data. Comparing them with the dotted and dashed curves, make it clear that the coupled-channels

effects can change strongly both the magnitudes and energy dependence of the $\pi N \to \pi\pi N$ cross sections.

To further see the dynamical content of our model, we show in Figs. 8 and 9 the contributions to the invariant mass distributions at $W = 1.79$ GeV from each of the processes via the final $MB = \pi\Delta, \rho N, \sigma N$ defined by Eqs. (5)–(7). The results shown in Figs. 8 and 9 indicate that the full coupled-channels calculations (solid curves) involve rather complex interference effects among these three unstable particle channels. To improve the model, we need to tune their relative importance.

Compared with all previous investigations, another feature of this investigation is our treatment of the N^* resonance amplitudes. These amplitudes are generated from 16 bare states, as given in Ref. [13], which are dressed by the nonresonant interactions, as required by the unitarity condition and defined by Eqs. (9)–(13). In Fig. 10, we compare the full results (solid curves) and that calculated from keeping only the nonresonant amplitudes (dashed curves) for the invariant mass distributions of $\pi^- p \to \pi^+\pi^- n$ at $W = 1.44, 1.60,$ and
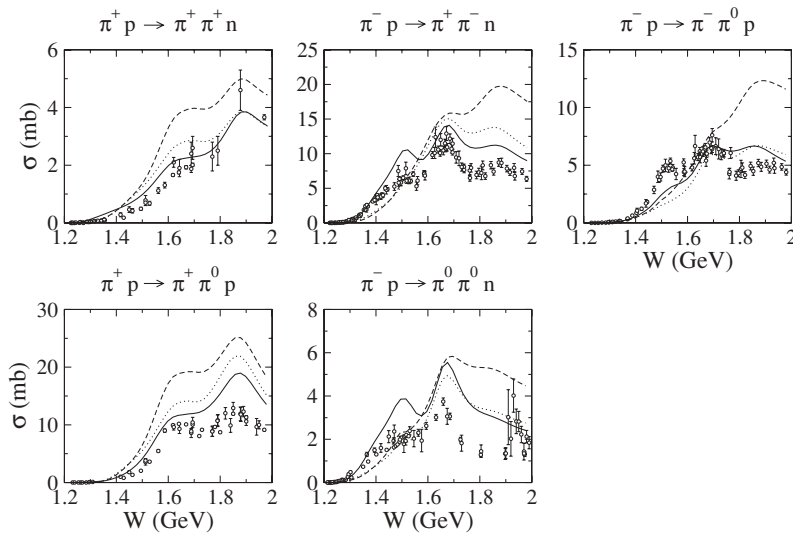

FIG. 5. The coupled-channels effects on $\pi N \to \pi\pi N$ reactions. The solid curves are from full calculations, the dotted curves are from keeping only $M'B' = MB$ in Eq. (36) and in $\bar{\Gamma}_{N^* \to MB}$ of Eqs. (12) and (13), and the dashed curves are from setting $t_{MB, M'B'} = v_{MB, M'B'}$. The data are from Ref. [31].

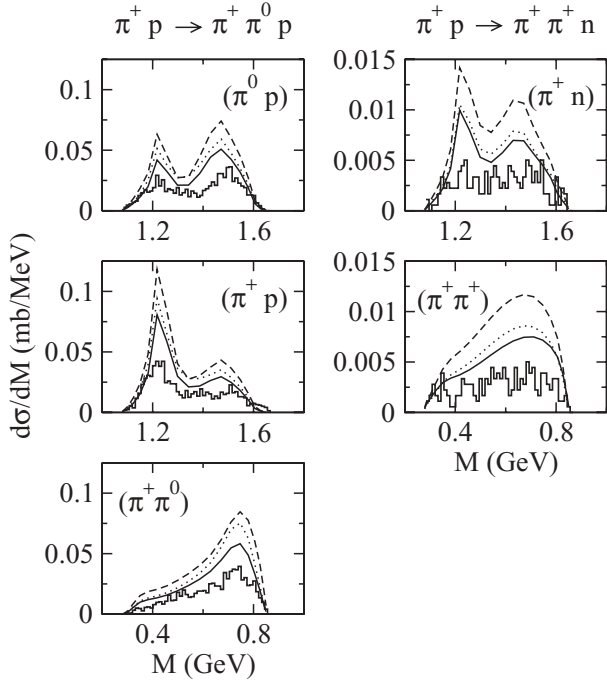FIG. 6. Coupled-channels effects on the invariant mass distributions of $\pi^+ p \to \pi\pi N$ at $W = 1.79$ GeV. The solid curves are from full calculations, the dotted curves are from keeping only $M'B' = MB$ in Eq. (36) and in $\bar{\Gamma}_{N^* \to MB}$ of Eqs. (12) and (13), and the dashed curves are from setting $t_{MB,M'B'} = v_{MB,M'B'}$. The data are from Arndt [30], with magnitudes determined by normalizing them to the total $\pi N \to \pi\pi N$ cross sections listed in Ref. [2].

FIG. 7. Coupled-channels effects on the invariant mass distributions of $\pi^- p \to \pi\pi N$ at $W = 1.79$ GeV. The solid curves are from full calculations, the dotted curves are from keeping only $M'B' = MB$ in Eq. (36) and in $\bar{\Gamma}_{N^* \to MB}$ of Eqs. (12) and (13), and the dashed curves are from setting $t_{MB,M'B'} = v_{MB,M'B'}$. The data are from Arndt [30], with magnitudes determined by normalizing them to the total $\pi N \to \pi\pi N$ cross sections listed in Ref. [2].

1.79 GeV. Here we note that the peaks of the dashed curves in $M(\pi^+ n)$ and $M(\pi^- n)$ distributions around 1.2 GeV in Fig. 10 are due to the decay of Δ in the intermediate $\pi\Delta$ state of the "nonresonant processes" of $\pi N \to \pi\Delta \to \pi\pi N$, whose amplitude is defined by Eq. (5) but replacing $T_{\pi N, \pi\Delta}$ with its nonresonant amplitude $t_{\pi N, \pi\Delta}$ generated from Eq. (14). Similarly, the decay of ρ (σ) in the intermediate ρN (σN) of the "nonresonant processes" of $\pi N \to \rho N(\sigma N) \to \pi\pi N$ can be responsible for the peaks of dashed curves in the $M(\pi^+ \pi^-)$ distributions (lower row of Fig. 10).

By comparing the solid and dashed curves in Fig. 10, it is clear that the full calculations involve comparable contributions from resonant and nonresonant amplitudes. In the same figure, we also show $\pi\pi N$ phase-space distributions (dotted curves) normalized to the data. The shapes of both theoretical results deviate significantly from the phase-space distributions.

The results shown in Fig. 10 indicate that the fits to the data depend strongly on the parameters associated with the $N^* \to \pi\Delta, \rho N, \sigma N$ vertex functions, which are treated purely phenomenologically within the JLMS model. One possible improvement of the model is to explore how these vertex functions can be calculated from sound hadron structure calculations. An attempt along this line for a two-channel πN scattering in the S_{11} state was pursued in Ref. [34] using the constituent quark model but was not successful.

The complexity of the calculated resonant amplitudes can be further seen in Table I, where we show the calculated
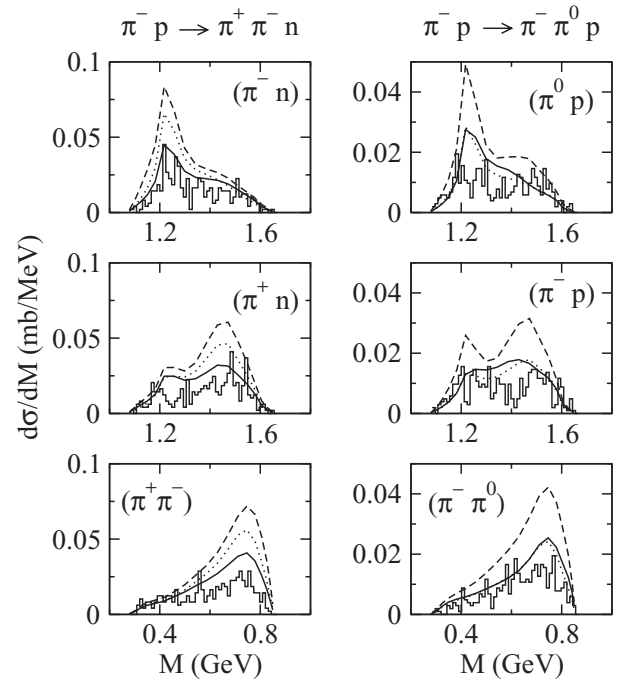

FIG. 8. Contributions from $\pi\Delta$ (dashed) and ρN (dot-dashed) channels to the invariant mass distributions of $\pi^+ p \to \pi\pi N$ at $W = 1.79$ GeV. The data are from Arndt [30], with magnitudes determined by normalizing them to the total $\pi N \to \pi\pi N$ cross sections listed in Ref. [2].
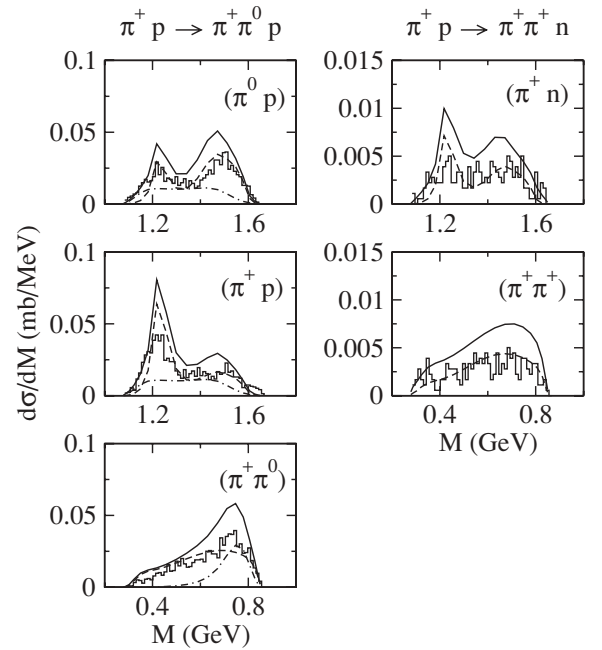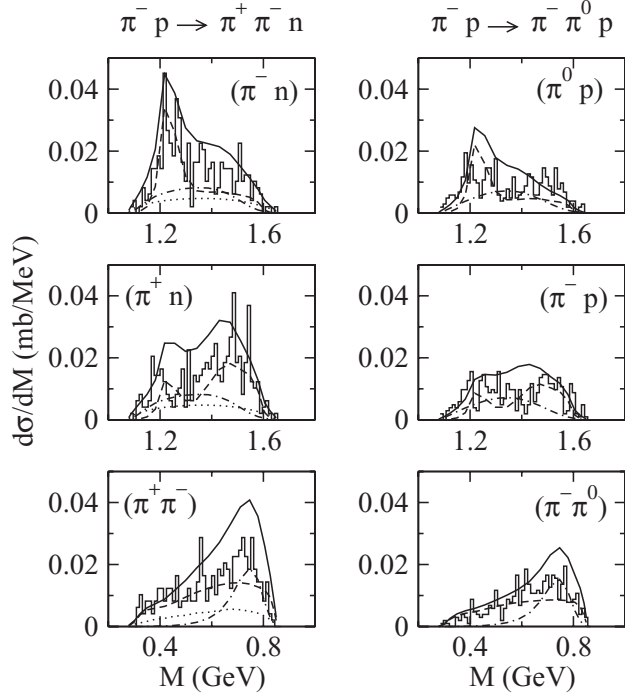
FIG. 9. Contributions from $\pi\Delta$ (dashed), σN (dotted), and ρN (dot-dashed) channels to the invariant mass distributions of $\pi^- p \to \pi\pi N$ at $W = 1.79$ GeV. The data are from Arndt [30], with magnitudes determined by normalizing them to the total $\pi N \to \pi\pi N$ cross sections listed in Ref. [2].

TABLE I. Branching ratios of the $\pi N \to \pi N$, ηN, $\pi\Delta$, σN, ρN partial wave cross sections calculated from the resonant amplitude [Eq. (9)]. W is the total energy.

States	W (MeV)	$\frac{\sigma_{MB}}{\sigma_{\text{total}}}$ (%)				
		πN	ηN	$\pi\Delta$	σN	ρN
S_{11}	1535	50.7	34.9	8.0	6.1	0.3
	1650	72.3	4.0	1.1	8.2	14.4
S_{31}	1620	26.6	0	67.3	0	3.1
P_{11}	1440	62.5	0	7.7	29.5	0.3
	1710	51.2	2.0	8.23	24.6	14.0
P_{13}	1720	27.9	0.2	70.2	0.9	0.8
P_{31}	1910	79.5	0	6.0	0	14.4
P_{33}	1232	100	0	0	0	0
	1600	76.4	0	13.6	0	10.0
D_{13}	1520	58.0	0.0	36.8	4.5	0.8
D_{15}	1675	38.6	0.7	56.5	0.7	3.5
D_{33}	1700	12.4	0	85.2	0	2.4
F_{15}	1680	70.0	0.0	4.8	19.3	5.8
F_{35}	1905	10.9	0	51.1	0	38.0
F_{37}	1950	39.8	0	59.7	0	0.5

branching ratios of the contributions from each channel to the partial-wave cross sections calculated from the resonant amplitude $t^R_{\pi N, MB}$ [Eq. (9)] at the resonant energies

listed by the PDG. Clearly, the resonant amplitudes involve strong interference among the $\pi N \to \pi\Delta$, ρN, $\sigma N \to \pi\pi N$ amplitudes. To improve the model, we need to tune their relative importance. Clearly more detailed data, such as the single or double angular distributions and polarizations, are needed to make significant progress. We emphasize here that the results listed in Table I are *not* the branching ratios of $N^* \to MB$ decay widths at the resonance poles; these widths

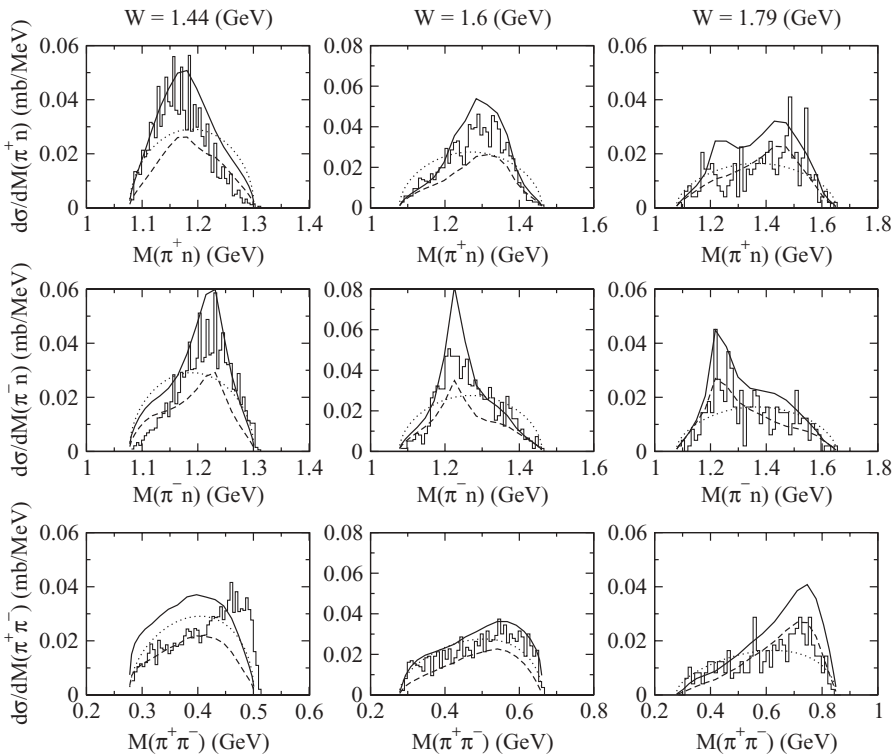FIG. 10. The invariant mass distributions of $\pi^- p \to \pi^+\pi^- n$ at $W = 1.44$, 1.60, and 1.79 GeV. The solid curves are the full calculations, the dashed curves are from nonresonant amplitudes, and the dotted curves are phase-space normalized to the data. The data are from Arndt [30], with magnitudes determined by normalizing them to the total $\pi N \to \pi\pi N$ cross sections listed in Ref. [2].
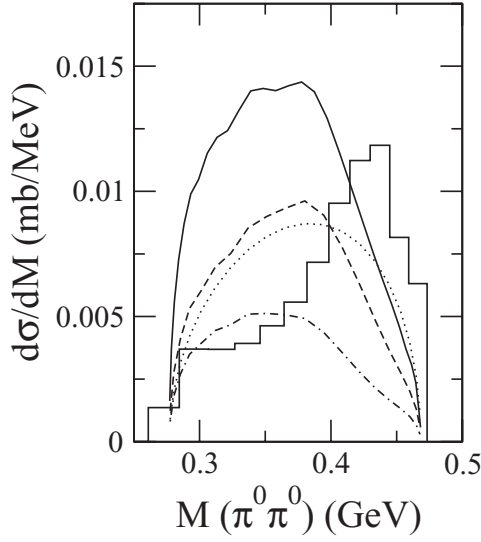
FIG. 11. The invariant mass distributions of $\pi^- p \to \pi^0 \pi^0 n$ at $W = 1.40$ GeV. The solid curve is the full calculation, the dashed (dot-dashed) curve is from keeping only the nonresonant (resonant) amplitude in the calculations, and the dotted curve is phase-space normalized to the data. The data are from Ref. [36]. (The data are transformed to $d\sigma/dM$ by using the relation $d\sigma/dM = 2M d\sigma/dM^2$.)

will be extracted from using the analytic continuation methods developed in Ref. [35]. The results here just give some idea of the relative importance of different channels at some energies listed by the PDG.

In Fig. 10, we also observe that our predictions do poorly in describing the $\pi^+\pi^-$ distribution at low W ($W = 1.44$ GeV). We have found that this is the case for all two-pion invariant mass distributions of $\pi^- p \to \pi^+ \pi^- n$ and $\pi^- p \to \pi^0 \pi^0 n$ reactions at $W \lesssim 1.5$ GeV. This is given in more detail in Fig. 11 for the $\pi^- p \to \pi^0 \pi^0 n$ reaction. We see that our prediction (solid curve) does not reproduce the data from the Crystal Ball Collaboration [36]. We also show the results from keeping only the nonresonance amplitudes (dashed curve) and only the resonant amplitude (dot-dashed curve). The shapes of all theoretical curves are similar to phase space (dotted curve) and are far from the data. We have found that the problem cannot be easily resolved by simply adjusting N^* parameters, in particular those in the most controversial P_{11} partial waves. Its resolution requires detailed analysis and more extensive $\pi N \to \pi \pi N$ data.

V. SUMMARY

In this paper we have shown that the predictions from the JLMS model can describe to a rather large extent the data of total cross sections and πN and $\pi \pi$ invariant mass distributions of $\pi N \to \pi \pi N$ reactions in the energy region from threshold to $W = 2$ GeV. Our investigation is thus more extensive than all previous dynamical calculations of this reaction in both the energy range covered and the N^* states considered.

We have demonstrated the importance of the coupled-channels effects and strong interference among the $\pi \Delta$, ρN, and σN channels. The problem in identifying the mechanisms for improving the considered JLMS model is further complicated by the finding that the contributions from resonant and nonresonant amplitudes are comparable.

An important finding in this work is that the direct $v_{\pi N, \pi \pi N}$ mechanisms, illustrated in Fig. 2, play a significant role in obtaining good agreement with the data, especially in the $W \leqslant 1.4$ GeV region where our results are comparable to those from chiral perturbation theory calculations [25–27]. This raises the questions of the extent to which our elastic scattering results will be changed by the effect from $v_{\pi N, \pi \pi N}$ and how the unitarity condition is violated. The former cannot be answered easily since it will involve solving three-body $\pi \pi N \to \pi \pi N$ scattering equations, as discussed in Ref. [12]. We however can examine the unitarity condition by comparing the total cross sections calculated from using (a) the optical theorem $\sigma_{\text{opt}}^{(\text{tot})} = (2\pi/k) F_{\pi N, \pi N}(\theta = 0)$, (b) $\sigma^{(\text{tot})} = \sigma_{\pi N, \pi N} + \sigma_{\pi N, \pi \eta} + \sigma_{\pi N, \pi \pi N}$ (with no $T_{\pi N, \pi \pi N}^{\text{dir}}$), and (c) $\sigma^{(\text{tot})} = \sigma_{\pi N, \pi N} + \sigma_{\pi N, \pi \eta} + \sigma_{\pi N, \pi \pi N}$. These are shown in Fig. 12. Here, $\sigma_{\pi N, \pi N}$ and $\sigma_{\pi N, \pi \eta}$ are directly calculated from the employed amplitudes generated from the JLMS model within which the effects of $v_{\pi N, \pi \pi N}$ are not included, and $\sigma_{\pi N, \pi \pi N}$ (with no $T_{\pi N, \pi \pi N}^{\text{dir}}$) and $\sigma_{\pi N, \pi \pi N}$ are calculated from using the formula given in Secs. II and III, with $T_{\pi N, \pi \pi N}^{\text{dir}}$ defined by $v_{\pi N, \pi \pi N}$ through Eq. (16). We see that (a) (solid curves) and (b) (dotted curves) agree completely, as required by the unitarity condition within the JLMS model. Their differences with (c) (dashed curves) measure the violation of the unitarity condition when the effects from $v_{\pi N, \pi \pi N}$ are not consistently included in solving the coupled-channels scattering equations. Clearly, the unitarity condition is violated significantly mainly in the high-W region. For example, the results for $\pi^- p$ total cross sections at $W = 1.8$ GeV are (a) 32.94 mb, (b) 32.48 mb, and (c) 35.57 mb. However, the results shown in Fig. 12 just mean that the effect of $v_{\pi N, \pi \pi N}$ will not change significantly the elastic differential cross sections at forward angles. For a complete unitary calculations for all
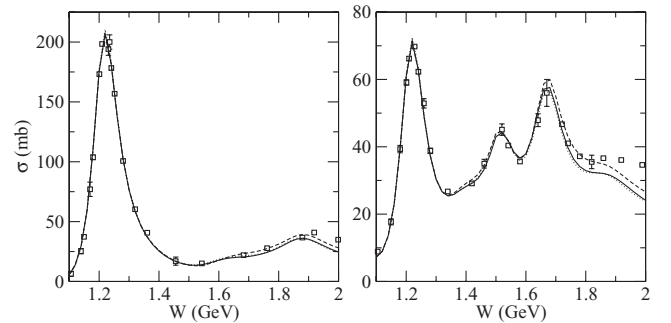

FIG. 12. Total cross sections of $\pi^+ p$ (left) and $\pi^- p$ (right) reactions calculated using the optical theorem $\sigma_{\text{opt}}^{(\text{tot})} = (2\pi/k) F_{\pi N, \pi N}(\theta = 0)$ (solid curves), $\sigma^{(\text{tot})} = \sigma_{\pi N, \pi N} + \sigma_{\pi N, \pi \eta} + \sigma_{\pi N, \pi \pi N}$ (with no $T_{\pi N, \pi \pi N}^{\text{dir}}$) (dotted curves), and $\sigma^{(\text{tot})} = \sigma_{\pi N, \pi N} + \sigma_{\pi N, \pi \eta} + \sigma_{\pi N, \pi \pi N}$ (dashed curves). Solid and dotted curves are not distinguishable. For a clear comparison of the curves, only a few data points are shown. The data are from Refs. [29,37].

πN reaction observables, we need to include $v_{\pi N, \pi\pi N}$ effects in solving the coupled-channels equations, as detailed in Ref. [12]. This is being pursued along with our effort in developing a combined fit to the world data of πN, $\gamma N \rightarrow \pi N$, ηN, $\pi\pi N$. Our progress in this direction will be reported elsewhere.

Our analysis presented in Figs. 6–11 indicates the complication of the $\pi N \rightarrow \pi\pi N$ problem. To improve our model, more experimental data, such as the single or double angular distributions and polarization observables, are needed to pin down the parameters of the model. With the recent effort by Arndt [30], progress in this direction could be realized in the near future. Of course, experimental efforts at the new hadron facilities such as JPARC are highly desirable.

ACKNOWLEDGMENTS

APPENDIX: SELF-ENERGY IN UNSTABLE *MB* PROPAGATORS

In this appendix we give a derivation of Eq. (35). To be more explicit, let us consider $eR = \pi\Delta$ for Eq. (35) and suppress spin-isospin indices. The starting point is Eq. (21) of Ref. [12], which defines the formulation used in the JLMS model and this work.

Since the vertex interaction $H_I = \Gamma_{\Delta, \pi N}$ conserves the total three-momentum of the system, we have

$$\left[\langle \vec{p}'_\Delta \vec{p}'_\pi | H_I \frac{P_{\pi\pi N}}{E - K_\pi - K_\pi - K_N + i\epsilon} H_I | \vec{p}_\Delta \vec{p}_\pi \rangle \right]_{\text{unconnected}}$$
$$= \delta(\vec{p}'_\Delta - \vec{p}_\Delta)\delta(\vec{p}'_\pi - \vec{p}_\pi)\Sigma_{\pi\Delta}(p_\pi, E). \quad \text{(A1)}$$

The kinematics for evaluating Eq. (A1) is illustrated in Fig. 13. To proceed further, we then use the following well-known relativistic kinematic relations (e.g., see Ref. [38] and Sec. 2.3 of Ref. [39]):

$$\vec{P} = \vec{k}_\pi + \vec{k}_N, \quad \text{(A2)}$$
$$\vec{q} = \frac{1}{2M_{\pi N}(E_{\pi N} + M_{\pi N})}$$
$$\times \left[(M_{\pi N}^2 + 2E_N(\vec{k}_N)M_{\pi N} + m_N^2 - m_\pi^2)\vec{k}_\pi \right.$$
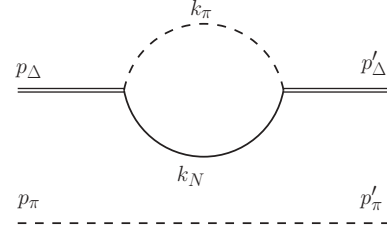

FIG. 13. Graphical illustration of Eq. (A1) for calculating the Δ self-energy in the $\pi\Delta$ propagator.

$$\left. - (M_{\pi N}^2 + 2E_\pi(\vec{k}_\pi)M_{\pi N} + m_\pi^2 - m_N^2)\vec{k}_N \right], \quad \text{(A3)}$$

with

$$E_{\pi N} = E_\pi(\vec{k}_\pi) + E_N(\vec{k}_N), \quad M_{\pi N} = E_\pi(\vec{q}) + E_N(\vec{q})$$
$$= \left[E_{\pi N}^2 - \vec{P}^2 \right]^{1/2}. \quad \text{(A4)}$$

We then have

$$d\vec{k}_\pi d\vec{k}_N = \left| \frac{\partial(\vec{k}_\pi, \vec{k}_N)}{\partial(\vec{P}, \vec{q})} \right| d\vec{P} d\vec{q}, \quad \text{(A5)}$$

with

$$\frac{\partial(\vec{k}_\pi, \vec{k}_N)}{\partial(\vec{P}, \vec{q})} = \frac{E_\pi(\vec{k}_\pi)E_N(\vec{k}_N)}{E_\pi(\vec{k}_\pi) + E_N(\vec{k}_N)} \cdot \frac{E_\pi(\vec{q}) + E_N(\vec{q})}{E_\pi(\vec{q})E_N(\vec{q})}$$
$$= \frac{E_\pi(\vec{k}_\pi)E_N(\vec{k}_N)}{E_\pi(\vec{q})E_N(\vec{q})} \cdot \frac{M_{\pi N}(q)}{\left[M_{\pi N}^2(q) + \vec{P}^2 \right]^{1/2}}. \quad \text{(A6)}$$

With the Lorentz invariance property [Eq. (27)], we can calculate the matrix element of H_I in terms of that in the rest frame of Δ:

$$\langle \vec{k}_\pi \vec{k}_N | H_I | \vec{p}_\Delta \rangle = \delta(\vec{p}_\Delta - \vec{k}_\pi - \vec{k}_N)$$
$$\times \sqrt{\frac{E_\pi(q)E_N(q)m_\Delta}{E_\pi(k_\pi)E_N(k_N)E_\Delta(p_\Delta)}} \langle \vec{q}, -\vec{q} | H_I | \vec{0} \rangle. \quad \text{(A7)}$$

By using these relations, we then have

$$\langle \vec{p}'_\Delta \vec{p}'_\pi | H_I \frac{P_{\pi\pi N}}{E - K_\pi - K_\pi - K_N + i\epsilon} H_I | \vec{p}_\Delta \vec{p}_\pi \rangle$$
$$= \delta(\vec{p}'_\pi - \vec{p}_\pi) \int \langle \vec{p}'_\Delta | H_I | \vec{k}_\pi \vec{k}_N \rangle$$
$$\times \frac{d\vec{k}_\pi d\vec{k}_N}{E - E_\pi(\vec{p}_\pi) - E_\pi(\vec{k}_\pi) - E_N(\vec{k}_N) + i\epsilon}$$
$$\times \langle \vec{k}_\pi \vec{k}_N | H_I | \vec{p}_\Delta \rangle. \quad \text{(A8)}$$

By using Eqs. (A5)–(A7), we then obtain

$$\langle \vec{p}'_\Delta \vec{p}'_\pi | H_I \frac{P_{\pi\pi N}}{E - K_\pi - K_\pi - K_N + i\epsilon} H_I | \vec{p}_\Delta \vec{p}_\pi \rangle$$
$$= \delta(\vec{p}'_\pi - \vec{p}_\pi) \int \left[\frac{E_\pi(q)E_N(q)m_\Delta}{E_\pi(k_\pi)E_N(k_N)E_\Delta(p_\Delta)} \right]$$
$$\times |\langle \vec{q}, -\vec{q} | H_I | \vec{0} \rangle|^2 \delta(\vec{p}'_\Delta - \vec{P})\delta(\vec{p}_\Delta - \vec{P})$$

$$\times \left[\frac{E_\pi(\vec{k}_\pi) E_N(\vec{k}_N)}{E_\pi(\vec{q}) E_N(\vec{q})} \cdot \frac{M_{\pi N}(q)}{[M_{\pi N}^2(q) + \vec{P}^{\,2}]^{1/2}} \right]$$

$$\times \frac{d\vec{q}\, d\vec{P}}{E - E_\pi(\vec{p}_\pi) - \{[E_\pi(\vec{q}) + E_N(\vec{q})]^2 + \vec{P}^{\,2}\}^{1/2} + i\epsilon}$$

$$= \delta(\vec{p}'_\pi - \vec{p}_\pi) \delta(\vec{p}'_\Delta - \vec{p}_\Delta) \frac{m_\Delta}{E_\Delta(p_\Delta)} \int \frac{M_{\pi N}(q)}{[M_{\pi N}^2(q) + \vec{p}_\Delta^{\,2}]^{1/2}}$$

$$\times \frac{d\vec{q}\, |\langle \vec{q}, -\vec{q} | H_I | \vec{0} \rangle|^2}{E - E_\pi(\vec{p}_\pi) - \left\{ [E_\pi(\vec{q}) + E_N(\vec{q})]^2 + \vec{p}_\Delta^{\,2} \right\}^{1/2} + i\epsilon}.$$

$$\text{(A9)}$$

Comparing Eqs. (A9) and (A1) and using the partial wave expansion [Eq. (28)], we then obtain in the center-of-mass frame ($\vec{p}_\pi = -\vec{p}_\Delta = \vec{k}$)

$$\Sigma_{\pi\Delta}(k, E)$$

$$= \frac{m_\Delta}{E_\Delta(k)} \int q^2 dq \frac{M_{\pi N}(q)}{[M_{\pi N}^2(q) + k^2]^{1/2}}$$

$$\times \frac{|f_{\Delta \to \pi N}|^2}{E - E_\pi(\vec{k}) - \{[E_\pi(\vec{q}) + E_N(\vec{q})]^2 + k^2\}^{1/2} + i\epsilon}.$$

$$\text{(A10)}$$

Equation (A10) is Eq. (35) for $eR = \pi\Delta$.

[1] V. Burkert and T.-S. H. Lee, Int. J. Mod. Phys. E **13**, 1035 (2004).

[2] D. M. Manley, R. A. Arndt, Y. Goradia, and V. L. Teplitz, Phys. Rev. D **30**, 904 (1984).

[3] D. M. Manley, Int. J. Mod. Phys. A **18**, 441 (2003).

[4] V. Shklyar, H. Lenske, U. Mosel, and G. Penner, Phys. Rev. C **71**, 055206 (2005).

[5] A. V. Anisovich, A. Sarantsev, O. Bartholomy, E. Klempt, V. A. Nikonov, and U. Thoma, Eur. Phys. J. A **25**, 427 (2005).

[6] T. P. Vrana, S. A. Dytman, and T.-S. H. Lee, Phys. Rep. **328**, 181 (2000).

[7] C. Schutz, J. Haidenbauer, J. Speth, and J. W. Durso, Phys. Rev. C **57**, 1464 (1998).

[8] O. Krehl, C. Hanhart, S. Krewald, and J. Speth, Phys. Rev. C **60**, 055206 (1999); **62**, 025207 (2000).

[9] W.-T. Chiang, F. Tabakin, T.-S. H. Lee, and B. Saghai, Phys. Lett. **B517**, 101 (2001).

[10] W.-T. Chiang, B. Saghai, F. Tabakin, and T.-S. H. Lee, Phys. Rev. C **69**, 065208 (2004).

[11] B. Juliá-Díaz, B. Saghai, T.-S. H. Lee, and F. Tabakin, Phys. Rev. C **73**, 055204 (2006).

[12] A. Matsuyama, T. Sato, and T.-S. H. Lee, Phys. Rep. **439**, 193 (2007).

[13] B. Juliá-Díaz, T.-S. H. Lee, A. Matsuyama, and T. Sato, Phys. Rev. C **76**, 065201 (2007).

[14] B. Juliá-Díaz, T.-S. H. Lee, A. Matsuyama, T. Sato, and L. C. Smith, Phys. Rev. C **77**, 045205 (2008).

[15] J. Durand, B. Juliá-Díaz, T.-S. H. Lee, B. Saghai, and T. Sato, Phys. Rev. C **78**, 025204 (2008).

[16] G. Y. Chen, S. S. Kamalov, S. N. Yang, D. Drechsel, and L. Tiator, Phys. Rev. C **76**, 035206 (2007).

[17] E. Oset and M. J. Vicente-Vacas, Nucl. Phys. **A446**, 584 (1985).

[18] O. Jakel, H.-W. Ortner, M. Dillig, and C. A. Z. Vasconcellos, Nucl. Phys. **A511**, 733 (1990).

[19] O. Jakel, M, Dillig, and C. A. Z. Vasconcellos, Nucl. Phys. **B541**, 675 (1992).

[20] O. Jakel and M. Dillig, Nucl. Phys. **A561**, 557 (1993).

[21] T. S. Jensen and A. F. Miranda, Phys. Rev. C **55**, 1039 (1997).

[22] H. Kamano and M. Arima, Phys. Rev. C **69**, 025206 (2004).

[23] H. Kamano and M. Arima, Phys. Rev. C **73**, 055203 (2006).

[24] V. Bernard, N. Kaiser, and U.-G. Meißner, Nucl. Phys. **B457**, 147 (1995).

[25] V. Bernard, N. Kaiser, and U.-G. Meißner, Nucl. Phys. **A619**, 261 (1997).

[26] N. Fettes, V. Bernard, and U.-G. Meißner, Nucl. Phys. **A669**, 269 (2000).

[27] N. Mobed, J. Zhang, and D. Singh, Phys. Rev. C **72**, 045204 (2005).

[28] S. Schneider, S. Krewald, and U.-G. Meißner, Eur. Phys. J. A **28**, 107 (2006).

[29] C. Amsler *et al.*, Phys. Lett. **B667**, 1 (2008).

[30] R. A. Arndt (private communications, 2008).

[31] G. Kernel *et al.*, Phys. Lett. **B216**, 244 (1989); G. Kernel *et al.*, *ibid.* **B225**, 198 (1989); J. Lowe *et al.*, Phys. Rev. C **44**, 956 (1991); S. Prakhov *et al.*, *ibid.* **69**, 045202 (2004); M. E. Sevior *et al.*, Phys. Rev. Lett. **66**, 2569 (1991); D. Počanić *et al.*, *ibid.* **72**, 1156 (1994); G. Kernel *et al.*, Z. Phys. C **48**, 201 (1990). The data before 1984 can be found in Ref. [2].

[32] T. Sato and T.-S. H. Lee, Phys. Rev. C **54**, 2660 (1996).

[33] J. A. Johnstone and T.-S. H. Lee, Phys. Rev. C **34**, 243 (1986).

[34] T. Yoshimoto, T. Sato, M. Arima, and T.-S. H Lee, Phys. Rev. C **61**, 065203 (2000).

[35] N. Suzuki, T. Sato, and T.-S. H. Lee, Phys. Rev. C **79**, 025205 (2009).

[36] S. Prakhov *et al.*, Phys. Rev. C **69**, 045202 (2004).

[37] CNS Data Analysis Center, GWU, http://gwdac.phys.gwu.edu.

[38] L. Heller, G. E. Bohannon, and F. Tabakin, Phys. Rev. C **13**, 742 (1976).

[39] B. D. Keister and W. N. Polyzou, Adv. Nucl. Phys. **20**, 225 (1991).